Optics Letters

Nonlinear frequency conversion and manipulation of vector beams

Haigang Liu,[1,2] Hui Li,[1,2] Yuanlin Zheng,[1,2] and Xianfeng Chen[1,2,*]

[1]State Key Laboratory of Advanced Optical Communication Systems and Networks, School of Physics and Astronomy, Shanghai Jiao Tong University, Shanghai 200240, China
[2]Key Laboratory for Laser Plasma (Ministry of Education), Collaborative Innovation Center of IFSA (CICIFSA), Shanghai Jiao Tong University, Shanghai 200240, China
*Corresponding author: xfchen@sjtu.edu.cn

Received 25 October 2018; revised 6 November 2018; accepted 10 November 2018; posted 12 November 2018 (Doc. ID 349213); published 7 December 2018

Vector beams have been extensively investigated in recent years because of their fascinating vector character across the beam transverse section, which is demonstrated to be useful for optical micro-manipulation, optical micro-fabrication, optical communication, single molecule imaging, and so on. To date, it is still a challenge to realize nonlinear frequency conversion and manipulation of such vector beams because of the polarization sensitivity in most nonlinear processes. Here, for the first time, to the best of our knowledge, we generate second-harmonic vector beams by using three-wave mixing processes in our experiment, which occur in two orthogonally placed nonlinear crystals, and the vector property is recognized by using a Glan–Taylor polarizer. This nonlinear frequency conversion process enables vector beams to be obtained at new wavelengths, and opens up new possibilities for all-optical switching and manipulation of vector beams. © 2018 Optical Society of America

https://doi.org/10.1364/OL.43.005981

Vector beams that have spatially inhomogeneous states of polarization in the transverse section of the beams are the solution to the vector Helmholtz equation [1]. It has been extensively investigated in recent years due to its fascinating vector characters. When a vector beam is tightly focused, its vector property can be used to tailor the optical field near the focus point. It has been demonstrated that a radially polarized beam can be tightly focused to generate a strong longitudinal and non-propagating electric field at the focal plane, resulting in a sharper focal spot than a homogeneously polarized beam [2]. Combining a specially designed diffractive optical element (DOE), a "pure" longitudinal light beam with subdiffraction beam size can be realized, which offers a way to break the diffraction limit in the far field [3]. In addition to a radially polarized beam, optical cages [4,5], optical needles [6], dark channels [7,8], optical chains [9], and top-hat beams [10] can also be realized by focusing other types of vector beams. More interestingly, optical orbital angular momentum (OAM) is also demonstrated from the curl of polarization in a hybrid polarized vector beam [11]. These attractive focusing properties are considerably important for many areas such as optical micro-manipulation [12,13] and optical micro-fabrication [14]. In optical communication areas, different space degrees of freedom of light beams can be used to increase communication capacity, which is known as space-division multiplexing (SDM). In recent years, despite a significant boost in research on applying OAM modes to increase the capacity of optical communication [15], spatially inhomogeneous polarization states, i.e., vector beams, have also been used in this interesting area [16,17]. Furthermore, it has been demonstrated that such vector beams can also be used in other physical systems, such as dynamic plasmonic beam shaping [18] and single molecule imaging [19].

Due to significant applications in the areas mentioned above, the generation and manipulation of such vector beams become more and more important. Different methods have been proposed to generate such vector beams. One method is by specially designing or modifying laser resonators [20,21] in some of the novel lasers. Another method is based on the wavefront reconstruction of traditional linear polarization lasers with the aid of specially designed optical elements [22]. Especially by using a spatial light modulator (SLM), the generation of such vector beams becomes more flexible [23,24]. However, all these studies have examined vector beams generated by linear diffractive elements. In previous research, more attention was paid on the nonlinear frequency conversion of vortex beams [25–27]. Although nonlinear generation of vector beams is reported by using metamaterials [28] and a nonlinear Cherenkov process in nonlinear photonic crystals [29], those works have problems of low efficiency and less flexibility. To date, it is still a challenge to realize nonlinear frequency conversion and manipulation of such vector beams. The vector property is wiped out when it has direct nonlinear frequency conversion because the phase-matching condition is polarization sensitive [30].

Here, we realize nonlinear frequency conversion and manipulation of vector beams for the first time by three-wave mixing (TWM) processes, taking place in two orthogonally placed quadratic nonlinear optical media. First of all, we generate the vector beams of fundamental frequency (FF) by a linear process in

which a SLM is used. And then, two orthogonally placed quadratic nonlinear crystals are used to convert the orthogonal polarization component of FF vector beams to the nonlinear waveband. In our experiment, the FF radially polarized vector beam and generated second-harmonic (SH) vector beam are analyzed, and the vector property across the beams' transverse section is recognized by a Glan–Taylor (GT) polarizer.

Step 1: generation of FF vector beam: the schematic of the experimental setup is shown in Fig. 1(a). The linearly polarized FF light is delivered from a Nd:YAG nanosecond laser with a wavelength of 1064 nm. A half-wave plate (HWP) and polarization beam splitter (PBS) are used to control polarization and intensity of the FF light. The SLM used in our experiments has a resolution of 1920 × 1080 pixels, each with a square area of 8 μm × 8 μm. It is divided into two parts: the first part is used to compensate the phase, and the second part, combined with a 45° quarter-wave plate (QWP), is used to change the polarization property of the beam. These two parts of the SLM are connected by a 4-f system, composed of a lens L_1 ($f_1 = 200$ mm) and a mirror. The Jose matrix of the first and second parts of the SLM can be, respectively, written as $M_{\mathrm{SLM1}} = \begin{pmatrix} \exp(i\delta_1) & 0 \\ 0 & 1 \end{pmatrix}$ and $M_{\mathrm{SLM2}} = \begin{pmatrix} \exp(i\delta_2) & 0 \\ 0 & 1 \end{pmatrix}$. Here, δ_1 and δ_2 are, respectively, the phase modulation function of the first and second parts of the SLM. The output of the optical field after passing through the QWP again can be calculated as

$$E(\omega) = M_{\mathrm{QWP}(135^\circ)} M_{\mathrm{reft}} M_{\mathrm{SLM2}} M_{\mathrm{QWP}(45^\circ)} M_{\mathrm{reft}} M_{\mathrm{reft}} M_{\mathrm{SLM1}} E_{\mathrm{in}} = \frac{1}{2}\exp(i\delta_1)\begin{pmatrix} 1-\exp(i\delta_2) \\ i(1+\exp(i\delta_2)) \end{pmatrix}. \quad (1)$$

When $\delta_1 = \pi - m\varphi - \varphi_0$ and $\delta_2 = 2(m\varphi - \varphi_0) - \pi$, the output of the FF optical field can be expressed as the form of the vector beam: $E(\omega) = [\cos(m\varphi + \varphi_0), \sin(m\varphi + \varphi_0)]$. Here, φ, m, and φ_0 are the azimuth angle, topological charge, and initial phase of the vector beams, respectively. Figure 1(b) represents the phase loaded on the SLM of the generated radially polarized FF vector beam.

Step 2: nonlinear frequency conversion of the vector beam: after the generation of the FF vector beam, another 4-f system is used to image it onto the sample shown in Fig. 1(a) to realize nonlinear frequency conversion. For simplicity and without loss of generality, the sample consists of two orthogonally placed 5 mol. % MgO:$LiNbO_3$ (LN) bulk crystals in our experiment. The two nonlinear crystals are cut for the Type I (oo-e) phase-matched process, as shown in Fig. 1(c1), and have the same thinness (1 mm) with orthogonal placed as illustrated in Fig. 1(c2) to ensure the same conversion efficiency of two orthogonal polarization components of the FF vector beams. Under paraxial and undepleted approximation of the FF beam, the coupled wave equation can be written as

$$\frac{dE_e(2\omega)}{dz} = \frac{i\omega d_{\mathrm{eff}}}{cn(2\omega)} E_o(\omega) E_o(\omega), \quad (2)$$

where $E_o(\omega)$, $E_e(2\omega)$, ω, d_{eff}, c, and $n(2\omega)$ are, respectively, the o-polarized component of incident FF vector beam, generated e-polarized SH, angular frequency of FF light, effective nonlinear coefficient, light speed in vacuum, and refractive index of SH. Supposing that o-polarized FF light is along x-polarized direction in the first and second nonlinear crystals shown in Figs. 1(c1) and 1(c2), the optical field of the generated SH can be written as

$$E(2\omega) = \frac{i\omega d_{\mathrm{eff}} L}{cn(2\omega)} \cdot \begin{pmatrix} \sin^2(m\varphi + \varphi_0) \\ \cos^2(m\varphi + \varphi_0) \end{pmatrix}, \quad (3)$$

where L represents the interaction distance or the length of one crystal. Therefore, arbitrary types of FF vector beams can be converted to SH vector beams, e.g., the radially polarized FF light converts into the SH vector beam, as shown in Fig. 1(d). Finally, an imaging system is used to record the optical intensity.

For simplicity and without loss of generality, SH generation of the FF radially polarized vector beam with topological charge $m = 1$ and initial phase $\varphi_0 = 0$ is realized. In this situation, the FF radially polarized vector beam and generated SH vector beam can be expressed as $E(\omega) = \{\cos[\varphi(x,y)], \sin[\varphi(x,y)]\}$ and $E(2\omega) \propto \{\sin^2[\varphi(x,y)], \cos^2[\varphi(x,y)]\}$, respectively. First

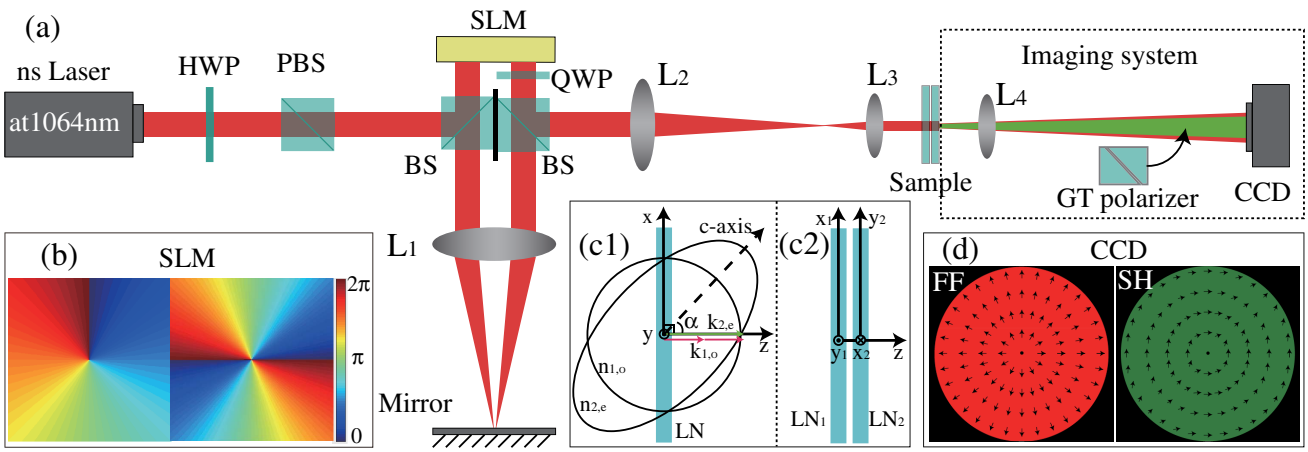

Fig. 1. (a) Schematic of the experimental setup. HWP, half-wave plate; BS, beam splitter; PBS, polarized BS; QWP, quarter-wave plate; SLM, spatial light modulator; $L_{1\text{–}4}$, lens, $f_{1\text{–}4} = 200$ mm, 200 mm, 50 mm, and 30 mm, respectively. Sample: two orthogonally placed quadratic nonlinear crystals. Without loss of generality, 5 mol. % MgO:$LiNbO_3$ (LN) is used in our experiment. (b) Phase loaded on SLM. (c1), (c2) Respectively, phase-matching type and relative position of two LN crystals (LN_1 and LN_2). (d) Polarization and intensity distribution of radially polarized FF vector beam and corresponding generated SH vector beam.

of all, we simulate the intensity and polarization distribution of the two vector beams in FF and SH wavebands, as shown in Figs. 2(a) and 2(b). A dark spot appears in the center of the beams, which arises from phase singularity. We can see that the intensity of the generated SH beam retains uniform distribution, and it still retains the vector property across the beam transverse section, as shown in Fig. 2(b). To illustrate the vector property of the vector beams in FF and SH wavebands, a GT polarizer is inserted into the light path before a CCD, as shown in Fig. 1. At this point the intensity distribution of the FF radially polarized vector beam and generated SH vector beam are, respectively, shown in Figs. 2(a1)–2(a9) and 2(b1)–2(b9). Polarization directions of the GT polarizer are, respectively, 0°, 20°, 40°, 60°, 80°, 100°, 120°, 140°, and 160° with respect to the positive horizontal direction and shown at the top right in Figs. 2(a1)–2(a9) and 2(b1)–2(b9). In the case of the FF radially polarized beam, we can see that the fanlike extinction position appears on the orthogonal polarization position of the GT polarizer and rotates with the changing of polarization direction of the GT polarizer, because of the changing of polarization states across the transverse section of the beam, as shown in Figs. 2(a1)–2(a9). In the case of the generated SH vector beam, completely extinction position appears in the horizontal direction after passing through the GT polarizer with 0° polarization direction, as shown in Fig. 2(b1). In this case, the orthogonal intensity distribution between the FF vector beam shown in Fig. 2(a1) and generated SH vector beam shown in Fig. 2(b1) arises from the oo-e phase-matching type in our experiments. The polarization state of the generated SH vector beam would be completely different if using a different phase-matching type. Rotating the polarization direction of the GT polarizer, the completely extinct position disappears until it reaches 90°, as shown in Figs. 2(b2)–2(b5), because no polarization state across the transverse section of the SH vector beam is strictly perpendicular to the polarization direction of the GT polarizer. More interesting, in this process, the intensity along vertical direction becomes lower and lower until reaching zero when the polarization direction of the GT polarizer reaches 90°. At the same time, intensity changes along horizontal direction are completely the contrary process. When we rotate the polarization direction of the GT polarizer more than 90°, two completely extinction position symmetric about the vertical direction would appear and continually close to the horizontal direction with the increasing of polarization angle of GT polarizer, as shown in Figs. 2(b6)–2(b9). Also, the intensity along horizontal direction becomes lower and lower until reaching zero when the polarization direction of the GT polarizer reaches 180°. At the same time, intensity changes along vertical direction are also the contrary process. We should point out that the intensity of SH along vertical direction is too weak to be observed in Figs. 2(b5) and 2(b6).

Next, the experimental results are shown in Fig. 3. In the case of the FF radially polarized beam, as shown in Fig. 3(a), the intensity is a uniform distribution, and the dark core in the center of the vector beam can be obviously observed. After passing through the GT polarizer, of which the polarization directions are the same as the theoretical simulations, the intensity distribution of the FF radially polarized vector beam is shown in Figs. 3(a1)–3(a9). It is easy to see that the experimental results are in good agreement with the theoretical simulations,

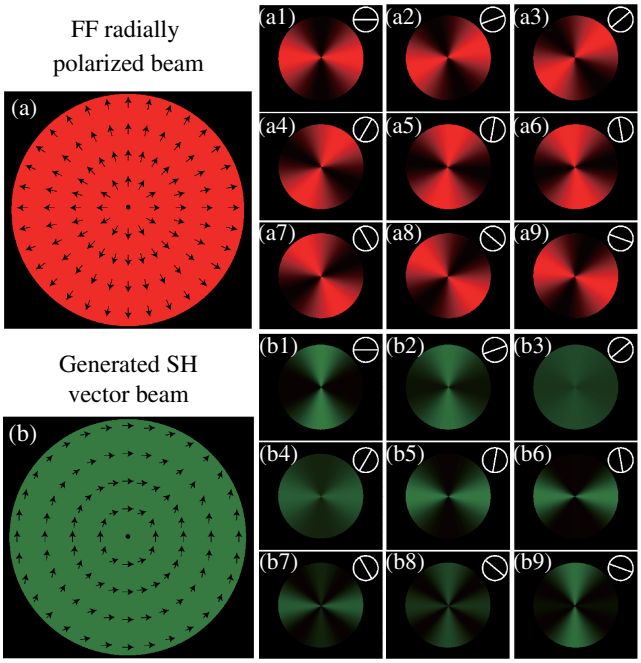

Fig. 2. (a), (b) Respectively, theoretical simulations of FF radially polarized vector beam and generated SH vector beam. (a1)–(a9) and (b1)–(b9) Respectively, intensity changes in FF radially polarized vector beam and generated SH vector beam for GT polarizer with different polarization directions (P = 0°, 20°, 40°, 60°, 80°, 100°, 120°, 140°, and 160°) shown at the top right of each figure added in the light path in Fig. 1.

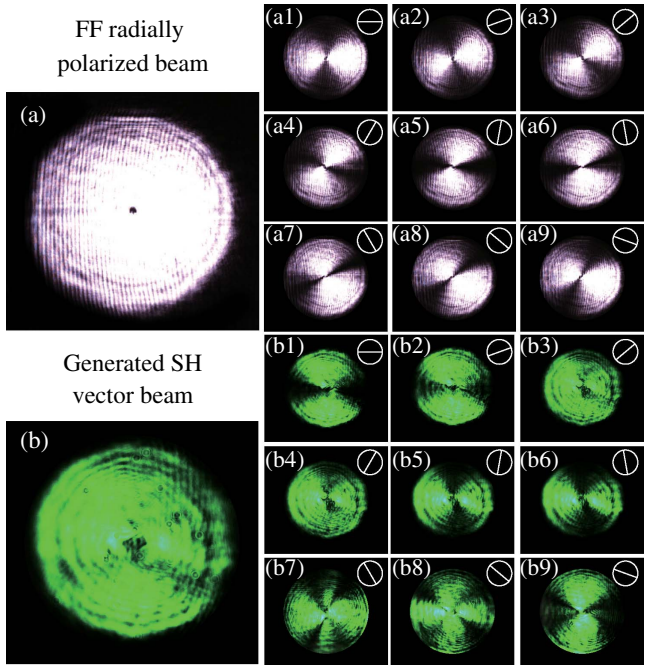

Fig. 3. (a), (b) Respectively, experimental results of FF radially polarized vector beam and generated SH vector beam. (a1)–(a9) and (b1)–(b9) Respectively, intensity changes in FF radially polarized vector beam and generated SH vector beam in the experiment for GT polarizer with different polarization directions (P = 0°, 20°, 40°, 60°, 80°, 100°, 120°, 140°, and 160°) added in the light path.

which are shown in Figs. 2(a1)–2(a9). The generated SH vector beam in the experiment is shown in Fig. 3(b). The imperfect experimental result compared to Fig. 2(b) is caused mainly by the diffraction of the FF and SH vector beams and the slight deviation of the relative position of two nonlinear crystals. After passing through the GT polarizer with different polarization directions, the intensity changes are shown in Figs. 3(b1)–3(b9), which is also in good agreement with the analysis of theoretical simulations shown in Figs. 2(b1)–2(b9).

In our experiment, the energies of one pulse of the input FF vector beam and generated SH vector beam are, respectively, 1 mJ and 3.8 μJ. The laser produces 4 ns pulses, and the repetition rate is 20 Hz. The radius of the FF vector beam is about 1.5 mm when it reaches the nonlinear crystals. Therefore, the conversion efficiency for peak power in the experiment is $1.52 \times 10^{-6}\%\ \mathrm{W}^{-1}$. The conversion efficiency would much higher if a longer nonlinear crystal were used, but its length should be shorter than the Rayleigh range of the FF vector beam to reduce the influence of beam diffraction.

The method presented here can be used to generate vector beams in arbitrary wavelengths by using different nonlinear processes, such as sum-frequency generation, difference frequency generation, and even the down-conversion process. Especially for the frequency range that modulation of the SLM cannot reach, the method we proposed still retains the dynamic and flexible property of the SLM. The vector beam has demonstrated its ability in the optical lithography area, which has a smaller focus spot and deeper penetration to the material [31]; therefore, the generation of ultraviolet vector beams by a high-harmonic process will extremely promote the optical lithography technique. Also, in optical communication areas, communication capacity by using a vector beam can be further improved by combining with wavelength-division multiplexing (WDM) technique. Hence, such nonlinear frequency conversion of vector beams provides a flexible way to realize this combination.

In conclusion, we realize nonlinear frequency conversion and manipulation of vector beams by TWM processes for the first time. Two orthogonally placed nonlinear crystals are used to convert the orthogonal polarization component of the FF vector beams to the nonlinear waveband. Theoretically, arbitrary types of FF vector beams can be converted to SH vector beams by using the method proposed here. For simplicity and without loss of generality, the FF radially polarized vector beam and generated SH vector beam are analyzed in our experiment. The vector property across the beam transverse section is recognized by a GT polarizer. Such a nonlinear frequency conversion process enables vector beams to be obtained at new wavelengths, and opens up new possibilities for all-optical switching and manipulation of vector beams.

Funding. National Key R&D Program of China (2017YFA0303700, 2018YFA0306300); National Natural Science Foundation of China (NSFC) (11734011); Foundation for Development of Science and Technology of Shanghai (17JC1400400).

REFERENCES

1. D. G. Hall, Opt. Lett. **21**, 9 (1996).
2. R. Dorn, S. Quabis, and G. Leuchs, Phys. Rev. Lett. **91**, 233901 (2003).
3. H. Wang, L. Shi, B. Lukyanchuk, C. Sheppard, and C. Chong, Nat. Photonics **2**, 501 (2008).
4. J. Arlt and M. J. Padgett, Opt. Lett. **25**, 191 (2000).
5. Y. Kozawa and S. Sato, Opt. Lett. **31**, 820 (2006).
6. J. Wang, W. Chen, and Q. Zhan, Opt. Express **18**, 21965 (2010).
7. Z. Chen and D. Zhao, Opt. Lett. **37**, 1286 (2012).
8. B. Tian and J. Pu, Opt. Lett. **36**, 2014 (2011).
9. Y. Zhao, Q. Zhan, Y. Zhang, and Y. Li, Opt. Lett. **30**, 848 (2005).
10. W. Han, W. Cheng, and Q. Zhan, Opt. Lett. **36**, 1605 (2011).
11. X. L. Wang, J. Chen, Y. Li, J. P. Ding, C. S. Guo, and H. T. Wang, Phys. Rev. Lett. **105**, 253602 (2010).
12. L. Huang, H. Guo, J. Li, L. Ling, B. Feng, and Z. Li, Opt. Lett. **37**, 1694 (2012).
13. G. Rui and Q. Zhan, Nanophotonics **3**, 351 (2014).
14. M. Meier, V. Romano, and T. Feurer, Appl. Phys. A **86**, 329 (2007).
15. J. Wang, J. Y. Yang, I. M. Fazal, N. Ahmed, Y. Yan, H. Huang, Y. X. Ren, Y. Yue, S. Dolinar, and M. Tur, Nat. Photonics **6**, 488 (2012).
16. G. Milione, M. P. J. Lavery, H. Huang, Y. X. Ren, G. D. Xie, T. A. Nguyen, E. Karimi, L. Marrucci, D. A. Nolan, and R. R. Alfano, Opt. Lett. **40**, 1980 (2015).
17. Y. Zhao and J. Wang, Opt. Lett. **40**, 4843 (2015).
18. Z. Man, L. Du, C. Min, Y. Zhang, C. Zhang, S. Zhu, H. P. Urbach, and X. Yuan, Appl. Phys. Lett. **105**, 011110 (2014).
19. L. Novotny, M. R. Beversluis, K. S. Youngworth, and T. G. Brown, Phys. Rev. Lett. **86**, 5251 (2001).
20. D. Naidoo, F. S. Roux, A. Dudley, I. Litvin, B. Piccirillo, L. Marrucci, and A. Forbes, Nat. Photonics **10**, 327 (2016).
21. Y. Kozawa and S. Sato, Opt. Lett. **30**, 3063 (2005).
22. K. C. Toussaint, S. Park, J. E. Jureller, and N. E. Scherer, Opt. Lett. **30**, 2846 (2005).
23. X. L. Wang, J. Ding, W. J. Ni, C. S. Guo, and H. T. Wang, Opt. Lett. **32**, 3549 (2007).
24. C. Maurer, A. Jesacher, S. Fürhapter, S. Bernet, and M. Ritsch-Marte, New J. Phys. **9**, 78 (2007).
25. S. M. Li, L. J. Kong, Z. C. Ren, Y. N. Li, C. H. Tu, and H. T. Wang, Phys. Rev. A **88**, 035801 (2013).
26. Y. Li, Z. Y. Zhou, D. S. Ding, and B. S. Shi, J. Mod. Opt. **63**, 2271 (2016).
27. Z. Y. Zhou, D. S. Ding, Y. K. Jiang, Y. Li, S. Shi, X. S. Wang, and B. S. Shi, Opt. Express **22**, 20298 (2014).
28. R. Camacho-Morales, M. Rahmani, S. Kruk, L. Wang, L. Xu, D. A. Smirnova, A. S. Solntsev, A. Miroshnichenko, H. H. Tan, F. Karouta, S. Naureen, K. Vora, L. Carletti, C. De Angelis, C. Jagadish, Y. S. Kivshar, and D. N. Neshev, Nano Lett. **16**, 7191 (2016).
29. S. M. Saltiel, Y. Sheng, N. Voloch-Bloch, D. N. Neshev, W. Krolikowski, A. Arie, K. Koynov, and Y. S. Kivshar, IEEE J. Quantum Electron. **45**, 1465 (2009).
30. L. Zhang, X. Qiu, F. Li, H. Liu, X. Chen, and L. Chen, Opt. Express **26**, 11678 (2018).
31. K. Kitamura, K. Sakai, and S. Noda, Opt. Express **18**, 4518 (2010).